

Superconductivity-enhanced conductance fluctuations in few-layer graphene

J Trbovic, N Minder, F Freitag and C Schönenberger

Department of Physics, University of Basel, Klingelbergstrasse 82, 4056 Basel, Switzerland

E-mail: jelena.trbovic@unibas.ch

Received 21 November 2009, in final form 18 January 2010

Published 22 June 2010

Online at stacks.iop.org/Nano/21/274005

Abstract

We investigate the mesoscopic disorder induced rms conductance variance δG in short few-layer graphene (FLG) flakes contacted by two superconducting (S) Ti/Al contacts. By sweeping the back-gate voltage, we observe pronounced conductance fluctuations superimposed on a linear background of the two-terminal conductance G . The linear gate voltage induced response can be modelled by a set of interlayer and intralayer capacitances. δG depends on temperature T and source–drain voltage V_{sd} . δG increases with decreasing T and $|V_{sd}|$. When lowering $|V_{sd}|$, a pronounced cross-over at a voltage corresponding to the superconducting energy gap Δ is observed. For $|V_{sd}| \lesssim \Delta$ the fluctuations are markedly enhanced. Expressed in the conductance variance G_{GS} of one graphene–superconductor (G–S) interface, values of $0.58e^2/h$ are obtained at the base temperature of 230 mK. The conductance variance in the sub-gap region is larger by up to a factor of 1.4–1.8 compared to the normal state. The observed strong enhancement is due to phase coherent charge transfer caused by Andreev reflection at the G–S interface.

(Some figures in this article are in colour only in the electronic version)

1. Introduction

Graphene nanostructures [1, 2] provide a unique opportunity to study fundamentally new quantum coherent phenomena and also possess an immense potential for applications [3]. The new quantum phenomena in graphene originate from the linear band structure of the relativistic-like quasiparticles and their chirality. The demonstration of a tunable supercurrent posed fundamentally new questions regarding the sources of apparent dephasing in this material since the amplitude of the critical current is lower than expected [4, 5]. Previous studies in disordered graphene devices [6–8] have shown that interference effects such as universal conductance fluctuation (UCF) and weak localization are dominant corrections to the conductance at low temperatures. First studies of UCF and weak localization were done in the 1980s in metallic systems and 2D semiconducting heterostructures [9]. Conductance fluctuations arising in these systems are universal, independent of sample size and the degree of disorder, reaching values of the order of e^2/h [9]. The interest in studying conductance fluctuations in graphene arose from predictions that they cease to be universal in the coherent state of disordered graphene [10]. In graphene samples a range of sources

of disorder have been identified: close proximity with the substrate [11], interaction with the leads [12, 13], rippling of the graphene layer [14], and unintentional doping. The disorder reduces the mobility of the quasiparticles. In the strong disorder regime, the variance of the conductance δG coincides with the predicted value for disordered metals, whereas in the weak disorder regime, δG is larger than the universal value due to the absence of back-scattering, characteristic of the honeycomb lattice of graphene [10]. Additional information on UCF in the system can be gained by attaching superconducting contacts to the disordered region [15]. At the interface between a normal metal N and a superconducting electrode S, phase sensitive Andreev reflections occur for energies lower than the superconducting energy gap Δ . At the N–S interface, an electron coming from N couples with its time-reversed counterpart to form a Cooper pair which can enter into S. The phase coherent Andreev states at the N–S interface can be destroyed by applying a magnetic field which breaks time reversal symmetry, by increasing the temperature, or by applying a large source–drain voltage.

In this work we study the two-terminal conductance of few-layer graphene (FLG) contacted by Ti/Al leads as a function of back-gate voltage V_g and source–drain voltage

V_{sd} . We find that the conductance variance increases with decreasing temperature, reaching an amplitude of the order of e^2/h at zero bias and a base temperature of 230 mK. By applying a source–drain voltage larger than Δ/e the conductance variance decreases by up to a factor of 1.8. A characteristic cross-over at an energy corresponding to Δ confirms that the observed enhancement is due to Andreev reflection at the graphene–S (G–S) interface. This finding complements existing work [7, 5, 8] by focusing on the bias dependence of conductance variance.

2. Sample fabrication and characterization

Graphene flakes were prepared by mechanical exfoliation of natural graphite (NGS GmbH, Leinburg, Germany) using a surface protection tape (SPV 224P from Nitto Denko), followed by the transfer of flakes onto a piece of highly p-doped Si wafer with a top thermal oxide layer of thickness $t = 304$ nm. The high doping of the substrate ensures the possibility to gate the flakes by applying a back-gate voltage V_g to the substrate. After flake transfer the samples were rinsed in solvents to remove the glue residue from the flakes and substrate. Suitable flakes were selected and localized by an optical microscope with respect to a grid of markers. The devices were patterned with e-beam lithography and subsequently metallized in an UHV e-beam evaporation system at a pressure of 10^{-7} mbar, followed by lift-off in acetone. In the present work we report results obtained from FLG devices contacted with superconducting aluminium (Al). In particular, we focus on short FLG having a contact separation that is shorter or comparable to the width. The sample for which we have the most complete data set and which we will discuss in detail in the following is shown in the inset of figure 1. This multi-layer flake was contacted with a Ti/Al/Ti tri-layer (5/40/20 nm). The purpose of the bottom Ti layer is to ensure high contact transparency between Al and graphene, whereas the top Ti layer caps the Al underneath. From the SEM image, we estimated the width W of the flake to be between 150 nm and 200 nm and the edge-to-edge distance L between the leads to be ~ 225 nm. A graphene sample which is much longer than wide serves as a control sample.

The back-gate dependence of the two-terminal linear differential conductance $G = dI/dV$ taken at 1.4 and 5.5 K (shifted by $0.2(2e^2/h)$ for clarity) in the range of $V_g \in [-10 \text{ V}, 50 \text{ V}]$ is shown in figure 1. Both traces were taken at temperatures where the contact leads are in the normal state. They show a minimum of the conductance $G_{\min} \approx 3.2e^2/h$ at 20 V, marking the position of the charge neutrality point (CNP). A small back-gate shift between the two curves of ≈ 2 V is observed after cooling the sample from 5.5 to 1.4 K. At 5.5 K the conductance linearly depends on V_g away from the CNP and shows small aperiodic, but reproducible, fluctuations. The amplitude of the fluctuations becomes larger after lowering the temperature to 1.4 K.

The magnitude of the conductance slope $\Delta G/\Delta V_g$ (marked with dashed lines in figure 1) can be used to estimate the number of layers N_L as demonstrated in the work of Zhang *et al* [16]. We have extended this model. Instead of a

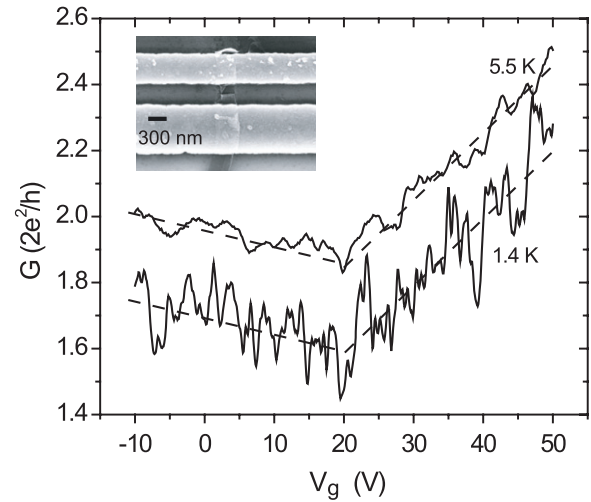


Figure 1. Two-terminal linear conductance G taken at 5.5 and 1.4 K as a function of the back-gate voltage V_g . The 5.5 K curve is shifted by $0.2(2e^2/h)$ to clearly show the increase of the conductance fluctuations upon lowering the temperature. The inset shows a scanning electron micrograph of the sample with Ti/Al/Ti electrodes across a few-layer graphene nanoribbon.

continuum we model the FLG as a discrete set of capacitively coupled conducting sheets (see appendix). Because of the strong electrostatic screening in the vertical direction of the FLG stack, the outermost carbon layer is affected most by the back-gate voltage. In the inner layers, in contrast, the electric gate field is strongly suppressed so that these layers add a nearly gate-independent conductance value proportional to the number of layers to the total conductance G . If one assumes that the electron diffusion constant is the same in all layers, an estimate for the number of layers N_L in the FLG can be obtained from the change in conductance $\Delta G/\Delta V_g$ normalized to the minimum conductance G_{\min} [16, 17]. Using our model, we estimate for the number of layers $N_L = 3\text{--}10$. We also obtain estimates for the charge carrier mobility μ , the electron diffusion constant D , and the elastic scattering mean free path l_e : $\mu \approx 140 \text{ cm}^2 \text{ V}^{-1} \text{ s}^{-1}$, $D \approx 17^2 \text{ s}^{-1}$, and $l_e \approx 3.5 \text{ nm}$.

3. Conductance measurements

Upon cooling the sample below the critical temperature of bulk Al, $T_c^{\text{bulk}} = 1.2 \text{ K}$, an energy gap $\Delta^{\text{bulk}} \approx 200 \mu\text{eV}$ opens in the density of states of Al. At the base temperature of 230 mK the transport properties of the device are deduced by measuring the two-terminal differential conductance G as a function of source–drain V_{sd} and back-gate voltage V_g , represented by the grey-scale plot in figure 2(a). The differential conductance G was obtained by superimposing an AC excitation voltage of $20 \mu\text{V}$ onto the DC part of the source–drain voltage and measuring the pre-amplified AC current with a lock-in amplifier. For each back-gate voltage in the range from -10 to 20 V V_{sd} is swept from -0.8 to 0.8 mV . In the grey-scale plot shown in figure 2(a) we observe a reproducible pattern of conductance fluctuations

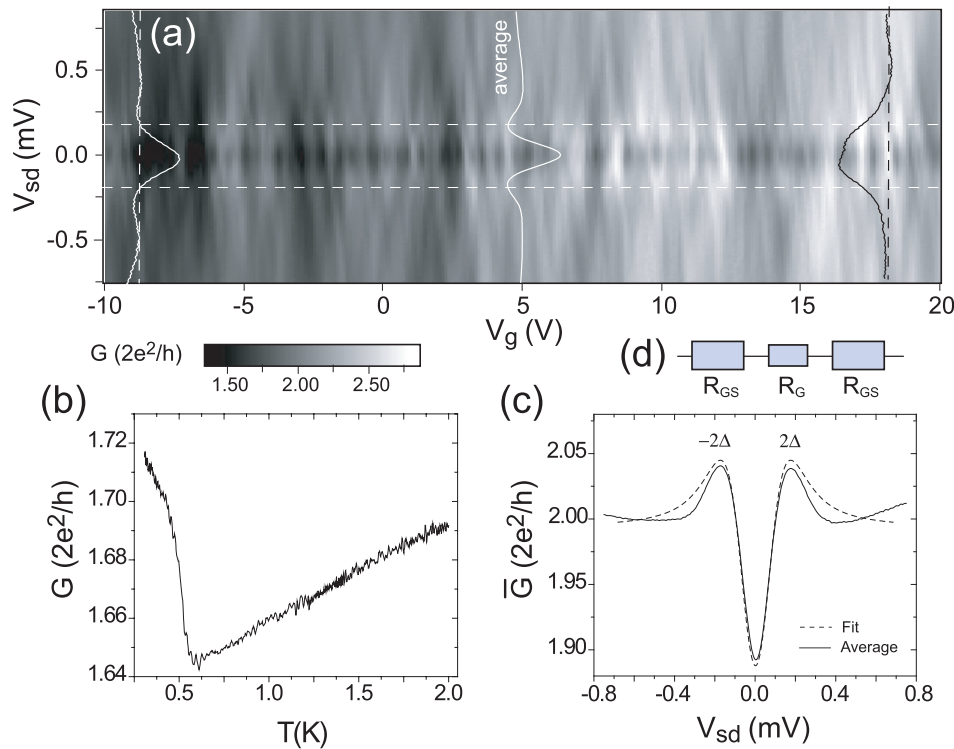


Figure 2. (a) Grey-scale plot of the two-terminal conductance $G = dI/dV$ as a function of the back-gate voltage V_g and the source–drain voltage V_{sd} at $T = 230$ mK. The dashed white lines indicate the position of twice the superconducting gap $2\Delta/e$. An example of a conductance spectrum with dip around zero bias is shown on the left, whereas one with a peak is shown on the right with the average curve placed in the middle of the plot. (b) Temperature dependence of the linear conductance taken during the sample cool-down at $V_g = 0$. (c) The conductance averaged over all back-gate curves $\overline{G}(V_{sd})$ as a function of V_{sd} . (d) In our system the interface resistances between the graphene and superconductor dominate over the internal resistance of the FLG. This is illustrated in the resistor network.

which is modulated by both V_g and V_{sd} . The amplitude of conductance fluctuations clearly diminishes as V_{sd} is increased. In contrast, as a function of back-gate voltage the fluctuations have a homogeneous amplitude, similar to what is seen in figure 1. As compared to the data in figure 1, the amplitude is larger in figure 2(a) due to the lower temperature. This dependence of conductance fluctuations points to so-called ‘universal conductance fluctuations’ (UCF), which are caused by quantum interference effects [9].

In addition to UCF, the presence of superconductivity is evident from the pronounced dark (low) conductance band around zero bias in between the 2Δ -lines, which are marked in figure 2(a) by white dashed lines. This band disappears at temperatures above the critical temperature T_c , as well as in a magnetic field larger than the critical field. The band of reduced conductance shows that the conductance is on average lower at low bias than it is at high bias (normal state). We illustrate this by overlaying the average conductance $\overline{G}(V_{sd})$ versus V_{sd} in the middle of the grey-scale plot. This, however, does not mean that all individual $G(V_{sd})$ curves show dips at zero source–drain voltage. Though the majority of $G(V_{sd})$ curves must display dips, such as the example overlaid on the left side of the grey-scale plot, there is a significant number of curves that display peaks around zero bias instead. An example is shown by the right overlaid curve (see also figure 3).

To quantify the energy scale at which the superconductivity related effects become important, we extract the critical

temperature T_c in the following. The conductance $G(T)$ as a function of temperature T was measured during the cool-down at $V_g = 0$. This is shown in figure 2(b). For this gate voltage value, $G(T)$ decreases with temperature, reaching a minimum at about 0.6 K. Below this temperature the conductance sharply increased, reaching a value of $1.72(2e^2/h)$ at the base temperature. We take the cross-over temperature at 0.6 K as the transition temperature T_c to the superconducting state. We note that the bulk value for Al is $T_c = 1.2$ K. The substantial reduction of T_c of 0.6 K in our superconductor–graphene–superconductor (S–G–S) device as compared to the bulk value may be due to the inverse proximity effect from the two normal metal Ti layers with thicknesses of 5 and 20 nm surrounding the Al [18].

Figure 2(c) shows the average conductance $\overline{G}(V_{sd})$ as a function of V_{sd} . This curve is obtained as the mean of all individual conductance curves measured at a fixed V_g value, after a small linear background was subtracted from the grey-scale plot in figure 2(a). In order to fit the data to the BTK model [19], we need to know how the voltage drops in our S–G–S device. To estimate this, we evaluate the resistor model shown in figure 2(d). The total resistance is divided into two interface–graphene resistors R_{GS} , which on both sides are taken to be equal, and the intrinsic resistance R_G of the FLG connected in series. We compare the measured minimum conductance G_{min} with the expected minimum conductivity σ_{min} of a single sheet of graphene. To do so, we will use the number of graphene layers in our FLG which we

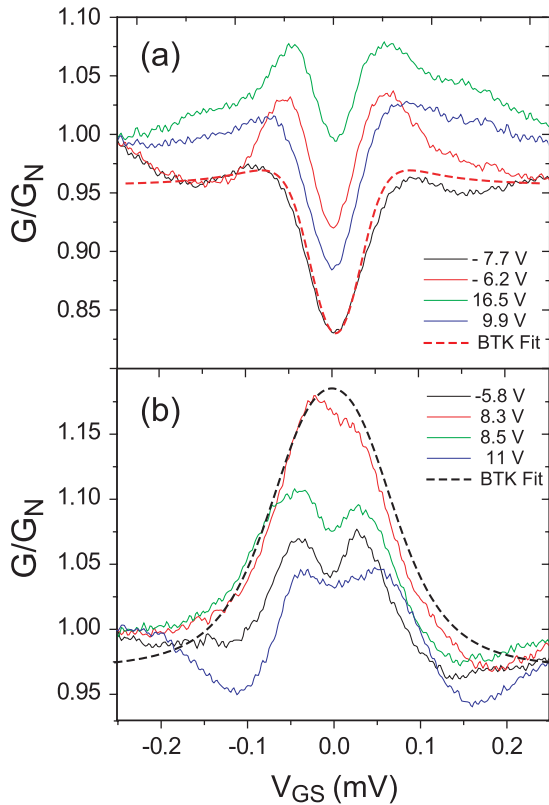


Figure 3. Typical differential conductance curves $G(V_{GS})$ for different constant back-gate voltages V_g displayed as a function of the voltage V_{GS} that drops over a single graphene–superconductor junction. $V_{GS} \simeq V_{sd}/2$. (a) In the bias window $|V_{GS}| < \Delta/e$ a dip is observed in $G(V_{GS})$ for $V_g = -7.7, -6.2, 16.5$, and 9.9 V, whereas (b) a peak appears for $V_g = -5.8, 8.3, 8.5$, and 11 V. All curves are normalized to the large bias conductance values G_N which are 1.76 (-7.7), 1.85 (-6.2), 2.44 (16.5), 2.38 (9.9), 1.92 (-5.8), 2.23 (8.3), 2.25 (8.5), 2.48 (11) in units of $2e^2/h$, where the number in bracket denotes V_g . The two BTK fits have the parameters $Z = 0.57$, $\Gamma = 22 \mu\text{eV}$ for the upper curve and $Z = 0.3$, $\Gamma = 10 \mu\text{eV}$ for the lower curve.

estimated in the previous section to be between 3 and 10. Unlike the electrons in a two-dimensional electron gas with quadratic dispersion, the Dirac electrons do not localize, not even for the smallest possible carrier density. Instead, there is a minimum conductivity σ_{\min} which is reached at the CNP. In experiments with graphene layers of intermediate disorder, σ_{\min} has been found to be $\approx 4e^2/h$ [20]. In the ballistic regime $\sigma_{\min} = (4/\pi)e^2/h$ has been predicted [21]. This value, which is reduced by a factor of π , has not yet been demonstrated experimentally, not even in the highest quality suspended graphene devices [22]. The estimate of the elastic mean free path in the previous section has shown that we are in the diffusive limit. In our experiment $G_{\min} \sim 3.2e^2/h$, which relates to $\lesssim 1e^2/h$ per layer. Since this value is appreciably smaller (by \approx a factor of 4) than σ_{\min} in the diffusive limit [20], the total resistance must be dominated by the interface resistances, i.e. $2R_{GS} > R_G$. Taking this into account, we simplify our network by dropping R_G altogether. We therefore assume that the applied source–drain voltage V_{sd} drops symmetrically over the source and drain contact. The

voltage drop V_{GS} across one interface is then half of the voltage V_{sd} applied across the junction, and hence $G_{GS} = 2G$.

We are now in the position to model the measured average conductance curve $\bar{G}(V_{sd})$ in figure 2(c) using the BTK model [23, 19]. This fit, which is shown in figure 2(c) by the dashed curve, provides as one parameter the superconducting energy gap $\Delta^{\text{av}} = 60 \mu\text{eV}$. Other fitting parameters deduced from the model are the effective barrier strength $Z \approx 0.6$ and an inelastic broadening parameter $\Gamma \approx 10 \mu\text{eV}$. Note that the barrier strength Z is related to the barrier transmission probability T according to $Z = \sqrt{1 - T^2}/T$. The broadening parameter is introduced as an imaginary energy term in the BCS density of states, $\rho(E, \Gamma) = (E - i\Gamma)/[(E - i\Gamma) - \Delta^2]^{1/2}$, with E being the energy of quasiparticles measured from the Fermi energy [23]. The superconducting energy gap Δ^{av} can be compared to the previously deduced transition temperature $T_c = 0.6$ K. Taking the BCS relation $\Delta = 1.76k_B T_c$ [18], one obtains $\Delta \approx 90 \mu\text{eV}$. Good agreement between the two numbers is found. The consistent numbers support our simplified approximation that most of the voltage drops over the S–G contacts.

Figure 3 provides examples of individual conductance curves $G(V_{GS})$ taken for different values of V_g . Note that V_{GS} is the voltage over one G–S junction and is taken to be half of V_{sd} . As we have emphasized before, $G(V_{GS})$ is suppressed on average in the sub-gap region for small source–drain voltages V_{sd} because the majority of curves show dips around zero V_{sd} . Examples of such curves are shown in figure 3(a) for back-gate values $V_g = -7.7, -6.2, 16.5$ and 9.9 V. However, a substantial number of curves show peaks. Examples are given in figure 3(b) taken at $V_g = -5.8, 8.3, 8.5$ and 11 V. This shows that Andreev reflection can dominate sub-gap transport at the G–S interface and thereby enhance G . After fitting individual curves to the BTK model [23, 19] (dashed lines in (a) and (b)), we extract a superconducting gap of $\Delta/e \approx 65 \mu\text{V}$, which agrees very well with $\Delta^{\text{av}} = 60 \mu\text{eV}$ deduced for the average curve before. The inelastic broadening parameter Γ ranges between 10 and $20 \mu\text{eV}$, and for the barrier strength Z we obtain ≈ 1 for curves with dips and ≈ 0.3 for traces with peaks. This agrees with the notion that the conductance of a S–N interface can be enhanced in the superconducting state, provided the interface transmission is sufficiently high, and hence, the barrier strength Z is sufficiently small.

We now turn our attention to the bias dependence of the conductance fluctuations. From the conductance data in figure 2 obtained at 230 mK we determine the rms conductance variance for a fixed source–drain voltage V_{sd} by a statistical average over all $G(V_g)$ values in the gate voltage range. We assume that the large gate voltage window provides a sufficiently large ensemble of different disorder configurations. In order to determine the rms variance δG a linear background has been subtracted from $G(V_g)$, leaving us with values $\Delta G(V_g)$ with a zero mean. The rms variance δG of the whole two-terminal device is then given by $\langle \Delta G^2 \rangle^{1/2}$. For comparison with theory it can be convenient to relate the conductance variance to one G–S interface, which we denote by δG_{GS} . If we assume that the two G–S contacts fluctuate

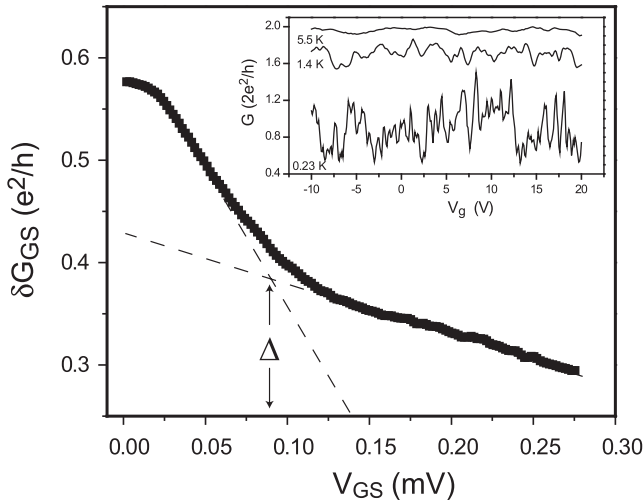


Figure 4. The conductance variance of a single graphene–superconductor (G–S) interface δG_{GS} (rms of the deviation of $G(V_{sd})$ relative to linear background times $\sqrt{2}$) as a function of the voltage drop across the G–S interface. $\delta G(V_{GS})$ displays a pronounced increase below a cross-over voltage that agrees with the superconducting gap value Δ . The inset displays $G(V_g)$ measured at different temperatures 5.5, 1.4 and 0.23 K, after subtracting a linear background for comparison. The 5.5 K curve is shifted by $0.2(2e^2/h)$ and the 0.23 K one by $-1.2(2e^2/h)$ for clarity.

independently $\delta G_{GS} = \sqrt{2}(\delta G)$. This is plotted in figure 4 as a function of voltage $V_{GS} = V_{sd}/2$ dropping over one contact.

In figure 4 we note two distinct regions with a clear cross-over at the energy $eV_{GS} \sim 90 \mu\text{eV}$ (arrow), which coincides with the previously estimated superconducting energy gap Δ of the Ti/Al/Ti tri-layer. In both regions δG_{GS} decreases with the applied bias. However, the decreasing rates of δG_{GS} are different for the two regions. In the high bias region, $V_{GS} > \Delta/e$, δG_{GS} decreases four times more slowly than in the region below the superconducting energy gap Δ . In the latter region, δG_{GS} starts saturating as the voltage drop across the junction V_{GS} approaches $k_B T/e \approx 20 \mu\text{V}$ and takes a finite value of $\delta G_{GS, 230 \text{ mK}} = 0.58e^2/h$ at zero bias. In addition, from the inset where conductance traces at 5.5 K, 1.4 K and 230 mK are shown, we find for the conductance variance at 1.4 K the value $\delta G_{GN, 1.4 \text{ K}} = 0.19e^2/h$ and at 5.5 K $\delta G_{GN, 5.5 \text{ K}} = 0.06e^2/h$, where the index N denotes that Al is in the normal state.

It is clear that the observed increase in δG_{GS} is due to the presence of the superconductor and Andreev reflections at the G–S interface. Our long control sample, which is as long as $1.5 \mu\text{m}$, does not show a cross-over but rather a smooth increase for decreasing V_{SD} . This is understandable, as the largest part of the voltage drop occurs in the bulk graphene and not at the two contacts. At zero temperature and zero magnetic field theory predicts an increase of 2.07 for the conductance variance of a single superconducting normal metal junction in the superconducting relative to the normal state [15]. A simple estimate provides from our data an enhancement of ≈ 1.4 , which is smaller than the maximum that can be expected. This estimate is obtained by linearly extrapolating δG from the high bias down to zero bias (lower dashed line in figure 4). This

extrapolation yields $\delta G = 0.3e^2/h$ for the variance δG of the whole two-terminal sample.

The reduced magnitude of the conductance variance ratio $\delta G_{GS}/\delta G_{GN}$ is not unexpected, taking the energy of the lowest temperature and the finite AC-bias modulation into account, which both lead to saturation of δG_{GS} at the lowest bias voltage in figure 4. The reduction of the saturation value δG from the expected ‘universal’ value can be caused by finite coherence. In the context of interference correction two parameters are important at zero magnetic field: the thermal length L_T and the phase-breaking length L_φ . The thermal length, sometimes also termed the coherence length, is given by $L_T = (\hbar D/k_B T)^{1/2}$. With $D = 17 \text{ cm}^2 \text{ s}^{-1}$, we obtain $L_T \approx 240 \text{ nm}$. At the lowest temperature, the device therefore crosses over into the fully coherent regime. Hence, the reduced value of δG must primarily originate from a finite phase-breaking length $L_\varphi < L$.

To compare further with theory, a value of $\delta G = 0.69\sqrt{W/L}e^2/h$ was predicted for a graphene ribbon with normal metal contacts [10]. For the geometry of our device this would translate into $\delta G \approx 0.6e^2/h$. Our estimated normal state δG value is two times smaller. This can be used to estimate an effective coherence length L_φ by using standard averaging along the length of the ribbon [24], yielding $G \sim 0.69\sqrt{W/L}(L_\varphi/L)^{3/2}e^2/h$. With L being 225 nm, we estimate a phase-breaking length of $L_\varphi \approx 80 \text{ nm}$ at 230 mK and consequently a phase-breaking time $\tau_\varphi \approx 4 \text{ ps}$.

The bias dependence of δG has not been studied systematically in G–S devices. However, some data are available in the literature. In recent experiments on a single graphene layer contacted with Pt/Ta superconducting leads the conductance variance at 60 mK was found to be $\delta G_{GS} = 2.4e^2/h$ [8]. Though this value is substantially larger than ours, a comparison has to take the larger width W into account ($W = 2.7 \mu\text{m}$ and $L = 330 \text{ nm}$). It turns out that also in this experiment the measured value is lower than the full coherence value, which we estimate to $4.3e^2/h$ using the expression $2.07 \times 0.69\sqrt{W/L}e^2/h$.

In nanostructures made of InAs nanowires contacted with Ti/Al leads [25–27] the saturation value of the conductance variance in the superconducting state was found to be $\sim 0.8e^2/h$ at 22 mK [25, 26] and $\sim 0.47e^2/h$ in the normal state, yielding an enhancement of ~ 1.6 , whereas in [27] at 300 mK $\delta G \sim 0.7e^2/h$ in the superconducting state was found with an enhancement factor of ~ 1.5 compared to the normal state. Both the normal state values and the enhancement factors for the superconducting state in these results are in good agreement with our observations in a Ti/Al contacted FLG.

In recent experiments with niobium contacted InAs nanowires a surprisingly large enhancement factor of ~ 30 was found [27]. The reason for such a strong enhancement is that the coherence length of the nanowire and the dephasing length L_φ is much larger than the distance between the contacts, so that multiple Andreev charge transfers which contribute to fluctuations can occur at the interface. The increased conductance variance signals the transition into the superconducting state of the whole device.

4. Summary and discussions

In conclusion, our measurements of FLG contacted with Ti/Al leads show pronounced UCF-type conductance fluctuations. We observe a decrease of the conductance variance with applied source–drain voltage with a characteristic cross-over for bias voltages corresponding to the superconducting energy gap Δ . For voltages below Δ/e the conductance variance is enhanced by a factor ranging between 1.4 and 1.8, which is close to the theoretically predicted value of 2.07. We think that the finite phase-breaking length $L_\varphi < L$, which compared to other works is relatively short, is the reason for the remaining discrepancy. We estimate L_φ to ≈ 80 nm at the base measurement temperature of 230 mK.

Acknowledgments

This work is financially supported by the NCCR on Nanoscale Science, the Swiss-NSF and EU-FP6-IST project HYSWITCH. We are grateful to the PSI (Paul Scherrer Institute) for the thermal oxidation of our Si wafers.

Appendix

In order to extract the number of graphene layers we extend the model of Zhang *et al* [16] by using a discrete capacitance model described in figure A.1(a). The back-gate is spaced by a distance t from an infinite set of graphene layers $j = 1, 2, 3, \dots$. The interlayer thickness between the graphene layers is taken to be d . E_j , Q_j , and ϕ_j denote the electrical field, the areal density of the excess charge measured from the CNP, and the electrostatic potential in the different graphene layers ($j \geq 1$) or back-gate ($j = 0$), respectively. For simplicity we set the dielectric constant to the vacuum permittivity ϵ_0 . This assumption can be relaxed afterwards by replacing the relevant parameter by the correct back-gate capacitance C_g . The difference in the electric fields is determined by the excess charge according to

$$Q_j = \epsilon_0(E_j - E_{j-1}). \quad (\text{A.1})$$

We assume that the graphene stack has a back contact (in our case realized by the source and drain contacts), which are set to zero, whereas the back-gate is biased to an electrochemical potential V_g . Because electrons can be exchanged between the different graphene layers by tunnelling, the electrochemical potentials of all layers are equal and zero in the thermodynamic limit. As a consequence the chemical potential μ_j of layer j is given by the negative of the electrostatic potential ϕ_j , i.e. $\mu_j = -e\phi_j$ with e the unit of charge. On the other hand, the chemical potential μ_j is determined by the excess charge density according to Q_j/eN_j , where the new symbol N_j denotes the areal density of states in graphene layer j . Taken together, we arrive at

$$\phi_j = -Q_j/e^2N_j. \quad (\text{A.2})$$

Adding for the charge Q_j the values given by (A.1), yields

$$\phi_j = \frac{\epsilon_0(E_{j-1} - E_j)}{e^2N_j}. \quad (\text{A.3})$$

A self-consistency relation can now be formulated by noting that the difference of the electrostatic potentials determines the electrical fields, i.e. $\phi_j - \phi_{j-1} = E_j d$. This leads to

$$E_j = \frac{\epsilon}{e^2Nd} \{E_{j+1} - 2E_j + E_{j-1}\}, \quad (\text{A.4})$$

where the density-of-states has been assumed to be constant and given by N . This equation has exponentially decaying solutions of the form

$$E_j = E_0 e^{-dj/\lambda}, \quad (\text{A.5})$$

where λ denotes the interlayer screening length. Placing (A.5) into (A.4) yields the following condition: $\cosh(d/\lambda) - 1 = e^2Nd/2\epsilon_0$. This equation determines the screening length λ . In order to quantify λ , the areal (two-dimensional) density-of-states N is required. We estimate N from the known three-dimensional value N_0 of graphite to $N = N_0 d$. With $N_0 = 5.2 \times 10^{20} \text{ cm}^{-3} \text{ eV}^{-1}$ and the interlayer distance $d = 0.34 \text{ nm}$ [28], one surprisingly obtains $d/\lambda \cong 1$, i.e. $\lambda \cong 0.34 \text{ nm}$. Eventually, we can place the solutions E_j in (A.5) back into the equations (A.2) and (A.3) to obtain the charge in layer j :

$$Q_j = -Q_0 e^{-(d/\lambda)(j-1)} \{1 - e^{-d/\lambda}\}. \quad (\text{A.6})$$

Obviously, if screening is strong ($\lambda \ll d$), $|Q_1| \simeq |Q_0|$, whereas $|Q_{j>1}| \ll |Q_0|$. In the opposite case of weak screening ($\lambda \gg d$), the charge decays slowly and is given for not too large j by $|Q_j| \simeq |Q_0|d/\lambda$. In the present situation with $\lambda \cong d$, 63% of the charge is in the first layer, 23% in the second, and the third layer already carries less than 10%. Hence, this model of an infinite stack of layers should work well for FLG stacks when the number of layers $N_L \gtrsim 3$. The parameter Q_0 in (A.6) can be related to the applied gate voltage V_g using the relation $\phi_0 - \phi_1 = V_g - \phi_1 = E_0 t$. We then arrive at a relation between the charge Q_0 on the gate and the gate voltage V_g :

$$Q_0 = \frac{V_g}{1/C_Q + 1/C_g}, \quad (\text{A.7})$$

where C_g is the geometrical gate capacitance and C_Q is an effective chemical capacitance (sometimes also termed quantum capacitance), both taken per unit area. C_Q is given by

$$C_Q = \frac{e^2 N}{1 - e^{-d/\lambda}}. \quad (\text{A.8})$$

Equation (A.7) shows that this relation represents a series connection of C_g with an effective quantum capacitance C_Q as depicted in figure A.1(b). The latter can also be derived from the circuit shown in figure A.1(c) consisting of an infinite series of interlayer capacitances C_i and intralayer quantum capacitances $C_q = e^2 N$ [29]. We next estimate the two capacitances C_g and C_q . Taking $\epsilon = 3.9$ for the relative permittivity of SiO_2 yields $C_g = 1.1 \times 10^{-4} \text{ F m}^{-2}$. With the aerial density of states N , which we estimated before from known graphite values, we obtain $C_q = 2.8 \times 10^{-2} \text{ F m}^{-2}$. Hence, $C_q \gg C_g$ by more than two orders of magnitude. Since the smaller capacitance counts in a series connection like as the one shown in figure A.1(b), the relation between gate charge

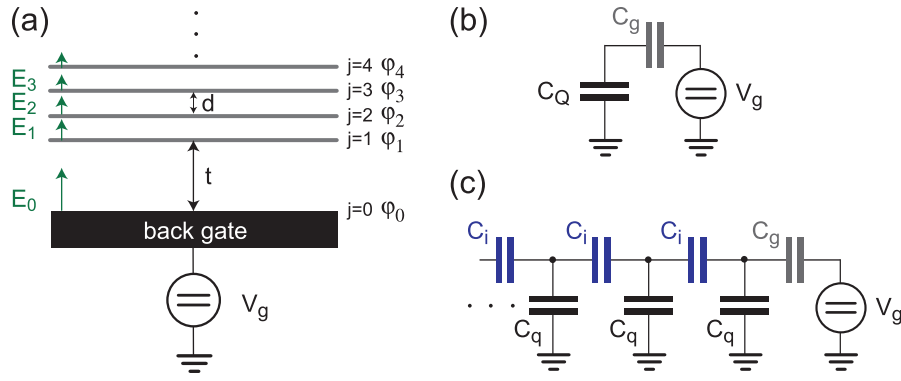


Figure A.1. (a) Schematics of the model to calculate the electric-field screening in a FLG stack which is gated by an electrostatic back-gate voltage V_g . E_j and ϕ_j denote the electric field and the electrostatic potential in layer j . (b) The circuit can be reduced to a series connection of two capacitances, where C_Q is an effective quantum capacitance and C_g the gate capacitance. (c) The full circuit diagram where C_g , C_i , and C_q denote the gate, graphite interlayer, and graphene intralayer capacitance, respectively. The latter capacitance is sometimes also termed quantum capacitance.

Q_0 and gate voltage V_g is to a very good accuracy given by the normal one $Q_0 \cong C_g V_g$.

Having analysed the screening problem, we can calculate the sheet conductivity of the whole stack. We assume it to be in the diffusive limit and use the Einstein equation, which relates the conductivity σ_j to the density-of-state in layer j and the diffusion constant D . In a Fermi gas the diffusion coefficient is given by $D = v_F^2 \tau / 2$, where v_F is the Fermi velocity, which in graphene is equal to 10^6 m s $^{-1}$, and τ the scattering time. For simplicity we assume that D is constant. This is an approximation, as it is known that there are surface effects and it is plausible that adsorbates might have the biggest effect on the mobility of the first layer. With this assumption we can write for the total conductance G of the FLG

$$G = \frac{W}{L} e^2 D \sum_{j=1}^{\infty} N_j, \quad (\text{A.9})$$

where W and L are the width and length of the FLG, respectively. The gate dependence of the conductance is due to the energy dependence in the density-of-states $N_j(E)$ which we now have to add here. In an ideal single graphene layer the energy dispersion relation is given by $E = \hbar v_F |\vec{k}|$, where \vec{k} denotes the wavevector in two dimensions. This dispersion results in a density-of-states N given by [16]

$$N(E) = \frac{2}{\pi} \frac{|E|}{(\hbar v_F)^2}. \quad (\text{A.10})$$

This density-of-states goes to zero for $E \rightarrow 0$. We have, however, assumed a finite density-of-states $N_0 d$ at the charge neutrality point (CNP; i.e. $E = 0$), which is caused by the interlayer overlap. To interpolate between the two regimes, we write:

$$N(E) = N_0 d + \frac{2}{\pi} \frac{|E|}{(\hbar v_F)^2} = N_0 d (1 + \beta |E|). \quad (\text{A.11})$$

The slope β is not a free parameter but is determined by the above equation. We obtain $\beta = 8.3$ eV $^{-1}$. Since the energy

E in (A.10) denotes the chemical potential, we can replace it with the electrostatic one. This leads together with (A.9) to:

$$G = \frac{W}{L} e^2 D N_0 d \sum_{j=1}^{\infty} (1 + \beta |e \phi_j|). \quad (\text{A.12})$$

Adding the explicit expressions for $\phi_j(V_g)$, the result is

$$G = \frac{W}{L} e^2 D N_0 d \left\{ N_L + (1 - e^{-d/\lambda})^{-1} \beta \frac{e V_g}{1 + C_q / C_g} \right\}. \quad (\text{A.13})$$

By dividing with the minimum conductance G_{\min} at $V_g = 0$, the dependence on the diffusion coefficient drops out. In the practical limit of $C_q \gg C_g$ the gate voltage change of G/G_{\min} is given by the final simple result:

$$\frac{\partial}{\partial V_g} \left(\frac{G}{G_{\min}} \right) = \frac{\beta e C_g}{N_L C_q}. \quad (\text{A.14})$$

We can apply this result to figure A.1. Equation (A.14) predicts a relative change of 3.3% V $^{-1}$ for $N_L = 1$. We measure a change of 1.2% V $^{-1}$ on the right and 0.32% V $^{-1}$ on the left. These two slopes correspond to $N_L = 3$ on the right and $N_L = 10$ on the left. The model clearly shows that we are dealing with a number of layers, but that we are in the regime of few layers with $N_L \lesssim 10$. Due to the different slopes for voltages smaller or larger than the CNP, a more accurate estimate for N_L cannot be given. However, we stress that physically we deal with one FLG with one given N_L number. The reduced change on the gate voltage to the left of the CNP suggests that the carrier density is markedly increased on the hole side, leading to an enhanced quantum capacitance. As the CNP is strongly on the positive side, the FLG is substantially hole doped. This hole doping may be caused by states that are induced by the source and drain contacts.

The dependence of conductance $G(V_g)$ on the gate voltage V_g can also be used to determine the mobility μ . Taking the derivative of equation (A.13) versus V_g and using the relation $C_q \gg C_g$ yields:

$$\frac{\partial G}{\partial V_g} = \frac{W}{L} D e \beta C_g. \quad (\text{A.15})$$

With the mobility μ one may also write the conductance as

$$G = \frac{W}{L} \mu Q, \quad (\text{A.16})$$

where Q is the effective carrier density. Since $C_q \gg C_g$, the gate voltage induced carrier density is given by $Q \cong C_g V_g = Q_0$. This leads to

$$\frac{\partial G}{\partial V_g} = \frac{W}{L} \mu C_g. \quad (\text{A.17})$$

By comparing this equation with equation (A.15), we deduce the relation $\mu = De\beta$. Taking the experimental value for $\Delta G/\Delta V_g \simeq 1.2e^2/h$ per 30 V, equation (A.17) provides a value of $\mu = 140 \text{ cm}^2 \text{ V}^{-1} \text{ s}^{-1}$ for the electron mobility. D then follows to be $\approx 17 \text{ cm}^2 \text{ s}^{-1}$, from which we estimate by virtue of $D = v_F l_e/2$ the scattering mean free path to $l_e \approx 3.5 \text{ nm}$. With $l_e < L, W$, we conclude that the device is diffusive, as anticipated at the beginning.

References

- [1] Novoselov K S, Geim A K, Morozov S V, Jiang D, Zhang Y, Dubonos S V, Grigorieva I V and Firsov A A 2004 *Science* **306** 666
- [2] Geim A K and Novoselov K S 2007 *Nat. Mater.* **6** 183
- [3] Geim A K 2009 *Science* **324** 1530
- [4] Heersche H B, Jarillo-Herrero P, Oostinga J B, Vandersypen L M K and Morpurgo A F 2007 *Nature* **446** 56
- [5] Du X, Skachko I and Andrei Eva Y 2008 *Phys. Rev. B* **77** 184507
- [6] Morozov S V, Novoselov K S, Katsnelson M I, Schedin F, Ponomarenko L A, Jiang D and Geim A K 2006 *Phys. Rev. Lett.* **97** 016801
- [7] Heersche H B, Jarillo-Herrero P, Oostinga J B, Vandersypen L M K and Morpurgo A F 2007 *Eur. Phys. J. Spec. Top.* **148** 27–37
- [8] Ojeda-Aristizabal C, Ferrier M, Guéron S and Bouchiat H 2009 *Phys. Rev. B* **79** 165436
- [9] Lee P A, Douglas Stone A and Fukuyama H 1987 *Phys. Rev. B* **35** 1039
- [10] Rycerz A, Tworzydło J and Beenakker C W J 2007 *Europhys. Lett.* **79** 57003
- [11] Chen S-H and Fuhrer Michael S 2008 *Nat. Nanotechnol.* **3** 206
- [12] Blake P, Yang R, Morozov S V, Schedin F, Ponomarenko L A, Zhukov A A, Grigorieva I V, Novoselov K S and Geim A K 2009 *Solid State Commun.* **149** 1068–71
- [13] Lee Eduardo J H, Balasubramanian Kannan, Weitz R T, Burghard M and Kern K 2008 *Nat. Nanotechnol.* **3** 486–90
- [14] Guinea F 2008 *Phys. Rev. B* **77** 205421
- [15] Beenakker C W J 1995 *Mesoscopic Quantum Physics* ed E Akkermans, G Montambaux, J-L Pichard and J Zinn-Justin (Amsterdam: North-Holland)
- [16] Zhang Y, Small Joshua P, Pontius William V and Kim P 2005 *Appl. Phys. Lett.* **86** 073104
- [17] Ihn T, Graf D, Molitor F, Stampfer C and Ensslin K 2008 *Physica E* **40** 1851–4
- [18] Tinkham M 2004 *Introduction to Superconductivity* (New York: Dover)
- [19] Blonder G E, Tinkham M and Klapwijk T M 1982 *Phys. Rev. B* **25** 4515
- [20] Novoselov K S, Geim A K, Morozov S V, Jiang D, Katsnelson M I, Grigorieva I V, Dubonos S V and Firsov A A 2005 *Nature* **438** 197–200
- [21] Tworzydło J, Trauzettel B, Titov M, Rycerz A and Beenakker C W J 2006 *Phys. Rev. Lett.* **96** 246802
- [22] Du X, Skachko I, Barker A and Andrei Eva Y 2008 *Nat. Nanotechnol.* **3** 491
- [23] Dynes R C, Narayanamurti V and Garno J P 1978 *Phys. Rev. Lett.* **41** 1509–12
- [24] Beenakker C W J and van Houten H 1991 *Solid State Phys.* **44** 1–228
- [25] Doh Y-J, De Franceschi S, Bakkers Erik P A M and Kouwenhoven Leo P 2008 *Nano Lett.* **8** 4098–102
- [26] Doh Y-J, Roest Aarnoud L, Bakkers Erik P A M, De Franceschi S and Kouwenhoven Leo P 2009 *J. Korean Phys. Soc.* **54** 135–9
- [27] Jespersen T S, Polianski M L, Soerensen C B, Flensberg K and Nygaard J 2009 arXiv:0901.4242
- [28] McClure J M 1957 *Phys. Rev.* **108** 612
- [29] Russ M, Meier C, Lorke A, Reuter D and Wieck A D 2006 *Phys. Rev. B* **73** 115334